Applied Catalysis B: Environmental 343 (2024) 123472

Contents lists available at ScienceDirect

Applied Catalysis B: Environmental

journal homepage: www.elsevier.com/locate/apcatb

Key role of material pore size in development of porous TiO_x electrodes for removal of organic compounds in flow-through reactor

Jing Ma [a], Clément Trellu [a,*], Nihal Oturan [a], Stéphane Raffy [b], Mehmet A. Oturan [a,*]

[a] Université Gustave Eiffel, Laboratoire Géomatériaux et Environnement, EA 4508, Cedex 2, Marne-la-Vallée 77454, France
[b] Saint-Gobain C.R.E.E., 550 Avenue Alphonse Jauffret, Cavaillon 84300, France

ARTICLE INFO

Keywords:
TiOx electrode
Porous material
Flow-through
Hydroxyl radicals
Anodic oxidation

ABSTRACT

Different porous TiO_x electrodes were synthesized for removing organic pollutants from water with a focus on the role of their porous structure on efficiency of electrocatalytic phenomena. In stirred-tank reactor, lower reaction rates were obtained using electrode with small pores (≈ 2.2 μm), while coarse roughness of electrodes with larger pores (≈ 100 μm) was beneficial. However, electrode with small pores allowed obtaining optimal mass transport in flow-through configuration. The reaction rate for degradation of 0.1 mM of terephthalic acid was 27 times higher compared to stirred-tank reactor. Reaction rates of electrodes with large pores were still limited from diffusion within pores and the reaction rate was divided by 2.8 at the optimal flux, compared to the electrode with small pores. A correlation was established between degradation yields, operating conditions and key characteristics of the porosity, which is crucial for the design of novel electrode materials with suitable porous structure.

1. Introduction

With the development of electrochemical technologies and applications in water treatment, many studies have been dedicated to promote the efficiency of anodic oxidation (AO) process for the removal of organic pollutants [1–8]. Electrode material and reactor design have attracted most attention, due to their crucial impact on the two most important factors of AO process: electrocatalytic formation of reactive species and mass transport conditions.

Dimensionally stable anodes (DSA), carbonaceous materials, metal oxides (e.g., PbO_2 and SnO_2), Pt and boron-doped diamond (BDD) have all been studied as anode material but each of them suffers from one or more drawbacks, including relatively low reactivity, low chemical resistance to corrosion, possible leaching of toxic metal ions or high cost [1,2,9–17]. In terms of reactivity, BDD constitutes an ideal anode material for the generation of physisorbed hydroxyl radicals ($^{\bullet}OH$) and subsequent non-selective destruction of organic pollutants [6]. However, some studies have shown that materials based on Magnéli phases (particularly Ti_4O_7 and Ti_5O_9) might be a promising alternative to BDD due to: (i) their high conductivity and suitable electrochemical reactivity for $^{\bullet}OH$ generation and (ii) their low cost since Ti is an abundant element on Earth [18–20]. Therefore, TiO_x electrodes are currently the focus of several studies on removal of different organic pollutants and decontamination of real wastewaters [21–27].

Reactor design and optimization of operating conditions is also catching much attention for improving mass transport conditions of organic pollutants from bulk to electrode surface. Flow-by reactors using plate electrodes aim at improving process efficiency by convection-enhanced mass transport that reduces the thickness of the diffusion boundary layer at the electrode/solution interface [28–32]. Further improvement has been obtained by the combination of filtration and anodic oxidation using flow-through reactors [33–36]. Therefore, the development of electrodes with suitable porous structure is currently an important challenge for obtaining efficient electrocatalytic materials for such applications [28,37–39].

Different TiO_x electrode materials have been synthesized and their effectiveness has been reported in literature. These TiO_x electrodes include dense and porous materials presenting different characteristics in terms of (i) nature of Magnéli phases obtained and (ii) porous structure/surface roughness [2,22,34,35,40–42]. However, it is still difficult to draw clear conclusions on the role of the porous structure of TiO_x electrodes for applications to the removal of organic compounds from water. Therefore, the objective of this study was to present the characteristics and reactivity of two 100% TiO_x materials with different porous

* Corresponding authors.
E-mail addresses: clement.trellu@univ-eiffel.fr (C. Trellu), mehmet.oturan@univ-eiffel.fr (M.A. Oturan).

https://doi.org/10.1016/j.apcatb.2023.123472
Received 25 June 2023; Received in revised form 9 October 2023; Accepted 5 November 2023
Available online 18 November 2023

structure. They were obtained either from carbothermal reduction of TiO_2 (small pores) (referred to as TiO_x SP) or from a foaming process of a TiO_x suspension (large pores) (referred to as TiO_x LP). Another electrode obtained from plasma spraying of TiO_x on a porous Ti substrate was used for comparison with the two 100% TiO_x porous electrodes. The investigation focused on: (i) the electrochemical reactivity for removal of organic compounds using probe molecules, (ii) the influence of reactor configuration, including stirred-tank and flow-through configurations, (iii) the correlation between material characteristics and process effectiveness and (iv) the identification of limiting phenomena among diffusion, convection and current supply according to material characteristics and operating conditions. The results obtained in this study provide new insights on the role of the porous structure of TiO_x materials for applications in the removal of organic pollutants from water by anodic oxidation process. Particularly, key characteristics of the porous structure are highlighted as regards to cell configuration. Conversion yields of target compounds are also correlated with key parameters related to electrode material reactivity, operating conditions (flow rate) and porous structure (specific surface area, thickness of the reaction zone).

2. Materials and methods

2.1. Chemicals

Terephthalic acid (≥99%) was obtained from Acros Organics. Oxalic acid (≥97%), sodium hydroxide (≥98%) and sodium sulfate (≥99%) were obtained from Fluka. Formic acid (≥96%) was provided by Sigma-Aldrich. Methanol (HPLC grade, ≥99.9%) was obtained from Honeywell Riedel-de-Haën. All chemicals were used as received without any purification. Ultrapure water (R>18.2 MΩ) obtained from a Smart2Pure device (Thermo Scientific, France) was used for the preparation of eluents for HPLC and ion chromatography.

2.2. Material synthesis

All the 100% TiO_x electrodes (100% TiO_x LP and 100% TiO_x SP) and Ti/TiO_x foam were provided by Saint-Gobain Research Provence, CREE.

100% TiO_x LP was synthesized according to the patent WO2006018537. TiO_x powders were mixed with gelling, foaming and stabilizing agents. The mixture was blended and sheared at temperatures higher than the gelation temperature of the gelling agent in order to obtain a foam. Then, the foam was cooled and dried to obtain a preform. Afterwards, discs were obtained using a slip casting method. Discs were then dried and sintered at 1450 °C under Ar (20 L h^{-1}) atmosphere for 2 h.

For 100% TiO_x SP, electrodes were obtained from uniaxial pressing of a mixture of 96.6% by weight of TiO_2 Anatase (ALTICHEM) and 3.4% by weight of Carbon Black Thermax 990 (CANCARB) to form a cylinder of 60 mm of diameter and 30 mm of height. Then, the cylinder was sintered at 1300 °C under Ar (20 L h^{-1}) atmosphere for 2 h. This step allowed for carbothermal reduction of TiO_2 to obtain the TiO_x phase and generate porosity within the material. A diamond wheel was used to cut porous discs with suitable dimensions.

The results obtained with 100% TiO_x electrodes were compared with a Ti/TiO_x foam, which was synthesized as presented in our previous study [40].

2.3. Material characterization

Porosity (for calculation details, please see the supporting information, Text SI-1), pore size distribution and specific surface area were analyzed by mercury intrusion porosimetry. The analysis was conducted on a Micromeritics porosimeter (AutoPore IV 9500 V1.06) with Hg contact angle of 140.9 degrees and Hg surface tension of 485 dynes cm^{-1}. The Hg intrusion pressure was set from 0.1 to 60000 psia. The chemical composition of 100% TiO_x electrodes was characterized by X-Ray diffraction (XRD). The analysis was conducted on a Bruker D8 ENDEAVOR diffractometer (Cu Kα radiation, λ = 1.5418 Å) at 40 kV and 40 mA. Database of PDF2–2004 (ICDD) was used for identification of TiO_x phases. Morphology and porous structure of 100% TiO_x electrodes were observed by a field emission electron probe microanalyzer (JEOL FEG JXA-8530 F) and a KEYENCE digital microscope (VHX-7000). Raman analysis was performed on a Renishaw inVia Raman microscope with solid-state green laser (Nd-YAG) at 532 nm with a laser energy filter set at 5% or 50%.

2.4. Electrochemical characterization

All electrochemical characterizations were performed on a Metrohm Autolab PGSTAT with a three electrodes system including a working electrode (100% TiO_x or Ti/TiO_x electrodes), a stainless steel as counter electrode and an Ag/AgCl/3 M KCl electrode as reference. Experiments were performed in 300 mL of 0.1 M $NaClO_4$ as supporting electrolyte.

Linear sweep voltammetry (LSV) tests were carried out from open circuit potential (OCP) to 3.8 V vs Ag/AgCl/3 M KCl at 0.01 V s^{-1} in order to study the electrode behavior for oxygen evolution reaction. Raw LSV data were corrected according to the uncompensated resistance of the electrochemical system [43–45]. Further details were provided in our previous study [40].

A method based on measurement of the double layer capacitance was used to calculate the electro-active surface area (EASA) [41]. Cyclic voltammetry (CV) tests were carried out at scan rate from 6 to 10 mV s^{-1} to calculate the double layer capacitance (as detailed in [40]). Then a specific capacitance of 60 μF cm^{-2} (typical for such material) was taken into consideration to calculate the EASA [41,46].

2.5. Experimental configurations for stirred-tank and flow-through reactors

A 400 mL cylindrical undivided stirred-tank reactor was operated in batch mode at a constant current density of 5 mA cm^{-2}. Ti/TiO_x foam and 100% TiO_x electrodes were used as anode. Carbon felt was used as cathode. Anode and cathode were placed face to face in the solution with an inter-electrode distance of 2.5 cm. The ratio between the geometric surface area of electrodes immersed in the solution and the volume of the solution was maintained constant at $S_{electrode}/V_{solution}$ = 7.9 m^{-1}. The solution was stirred using a magnetic bar at 750 rpm. Samples were taken from the reactor at different time intervals for analysis.

Flow-through experiments were performed in a glass reactor with $S_{electrode}$ = 12.6 cm^2. A porous TiO_x electrode was set at the bottom of the reactor as anode and a BDD with the shape of a grid was used at the top of the reactor as cathode for avoiding the accumulation of gas bubbles within the inter-electrode space. The solution was pumped from the feedwater reservoir through the reactor in dead-end filtration mode. Flow-through experiments were operated at constant current density of 5 mA cm^{-2} in continuous mode (single pass, 0% recirculation).

Despite the use of different materials as cathode, potential contribution of H_2O_2 (from O_2 reduction) to reaction mechanisms was neglected since (i) air/O_2 was not supply to the solution, (ii) H_2O_2 has low reactivity with target molecules used in this study. Schemes and pictures of the different configurations are provided in Supplementary Information (SI) file (Fig. SI-1).

2.6. Electrode reactivity assessment using probe molecules

Terephthalic acid (TA) has been reported as a suitable probe molecule for $^{\bullet}OH$ in an electrochemical system since it can be degraded only by $^{\bullet}OH$-mediated oxidation. Besides, oxalic acid (OA) has low reaction rates with reactive oxygen species, therefore it was used for monitoring an oxidation mechanism based on direct electron transfer (DET) [40,47,48]. 0.4 mM OA and 0.1 mM TA were used to have the same initial total

organic carbon (TOC) (9.6 mg L^{-1}). 50 mM Na_2SO_4 was used as supporting electrolyte. Reactivity tests were performed in both stirred-tank and flow-through reactors. In the flow-through reactor, degradation rate of probe molecules was studied according to the volumetric flow rate through the electrode.

Process effectiveness was assessed from calculated values of conversion yields (Eq. 1), mineralization yields (Eq. 2), conversion rates (g h^{-1} m^{-2}) (Eq. 3), mineralization rates (g h^{-1} m^{-2}) (Eq. 4) and energy consumption per log removal (EC) (kWh m^{-3}) (Eq. 5). Mineralization current efficiency (MCE) of OA and TA by different electrodes was calculated as detailed in our previous study [49].

$$conversion\ yield = \frac{C_{inlet} - C_{outlet}}{C_{inlet}} \quad (1)$$

$$mineralization\ yield\ (\%) = \frac{TOC_{inlet} - TOC_{outlet}}{TOC_{inlet}} \times 100 \quad (2)$$

$$conversion\ rate = (C_{inlet} - C_{outlet}) \times J \quad (3)$$

$$mineralization\ rate = (TOC_{inlet} - TOC_{outlet}) \times J \quad (4)$$

$$EC = \frac{I \times U}{J \times S \times \log\left(\frac{C_{inlet}}{C_{outlet}}\right)} \quad (5)$$

In these equations, C_{inlet} and C_{outlet} are concentrations of target molecule at the inlet and outlet of the flow-through cell, respectively, TOC_{inlet} and TOC_{outlet} are TOC concentrations at inlet and outlet of the flow-through cell, respectively, J is the volumetric flow rate (L h^{-1} m^{-2}), I is the current (A), U is the cell potential (V) and S is the geometric surface area of the electrode (m^2).

2.7. Analytical methods

TOC values in OA and TA solutions were assessed using a SHIMADZU TOC analyzer (TOC-L).

Concentration of TA and its degradation by-product HTA (2-hydroxyterephthalic acid) were analyzed by an Elite LaChrom HPLC system (HITACHI) coupled with a L-2400 UV detector (λ = 254 nm), a L-2480 fluorescence detector (Ex/Em=315/435 nm), a L-2130 pump (with a flow rate of 0.8 mL min^{-1}) and a LiChroCART Purospher® STAR RP-18e (5 μm) column set in a oven at 40 °C. The eluent was a mixture of methanol (40%) and 0.1% formic acid in water (60%).

3. Results and discussions

3.1. Material characterization

3.1.1. Pore size distribution

Results obtained from Hg porosimetry showed that 100% TiO_x LP has a median pore size of 127 μm as regards to pore volume (Fig. 1(a)) and 2.3 μm as regards to pore surface area. The porosity and specific surface area of 100% TiO_x LP were determined as 69% and 0.104 m^2 g^{-1}, respectively (Table 1). On the other hand, 100% TiO_x SP has median pore size of 2.2 μm as regards to pore volume (Fig. 1(b)) and 1.9 μm as regards to pore surface area. 100% TiO_x SP has a porosity of 29% and specific surface area of 0.202 m^2 g^{-1} (Table 1). Summary of Hg porosimetry analysis of the different TiO_x electrodes are presented in Table 1.

3.1.2. Porous structure

The porous structure of 100% TiO_x LP and SP was observed by a field emission electron probe microanalyzer (Figs. 2(a) and 2(b) for 100% TiO_x LP and SP, respectively) and a digital microscope (Figs. 2(c) and 2 (d) for 100% TiO_x LP and SP, respectively). 100% TiO_x SP presents a homogeneously interconnected and open porous structure with much smaller pore size compared to 100% TiO_x LP. As regards to 100% TiO_x LP, the open porous structure is mainly ascribed to large pores (which represent the main fraction of porous volume) while small pores are ascribed to small defects within the porous structure. These small pores participate to a little extent in water permeation. Therefore, median pore size calculated as regards to pore volume seems to be more appropriate for characterizing the effect of the porous structure on process effectiveness in flow-through configuration.

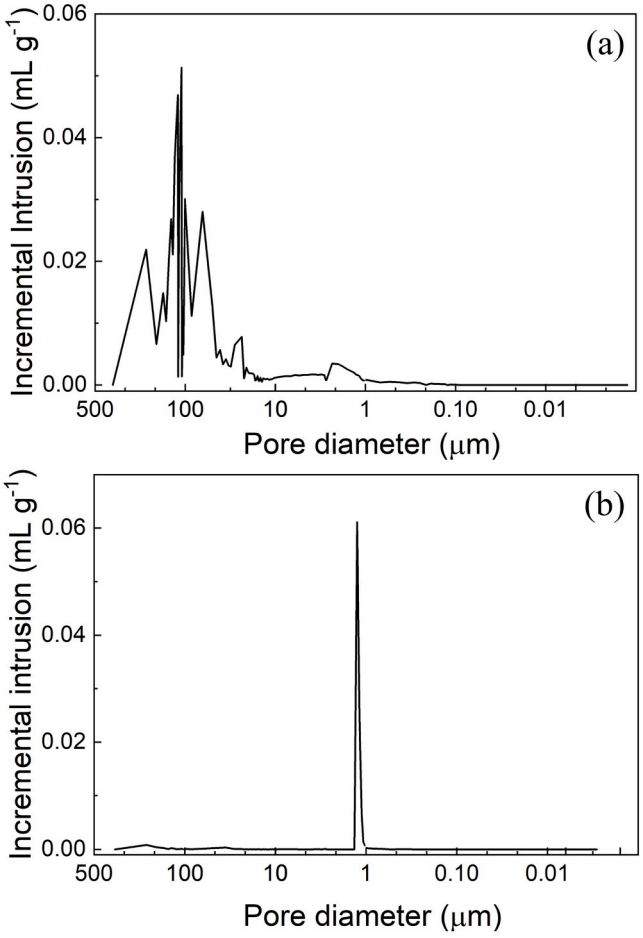

Fig. 1. Incremental intrusion volume of Hg according to pore diameter: 100% TiO_x LP (a) and 100% TiO_x SP (b).

Table 1
Hg porosimetry analysis of different TiO_x electrodes.

Electrode	Porosity	Specific surface area (m^2 g^{-1})	Median pore size (volume) (μm)	Median pore size (area) (μm)
Ti/TiO_x foam*	35%	0.013	88.0	15.2
100% TiO_x LP	69%	0.104	127	2.3
100% TiO_x SP	29%	0.202	2.2	1.9

* Data from Ma et al. (2022) [40]

The porous structure of Ti/TiO_x foam was already described in Ma et al. (2022). Data are given in SI (Fig. SI-2).

3.1.3. X-ray diffraction and Raman spectra

Chemical composition of 100% TiO_x electrodes was then assessed by XRD (Fig. 3). For both 100% TiO_x LP (Fig. 3(a)) and SP (Fig. 3(b)), the results indicate that the major phases were Ti_4O_7 and Ti_5O_9. Ti_6O_{11} was also detected as minor phase for 100% TiO_x SP. Different synthesis methods may lead to different stoichiometry of these Magnéli phases;

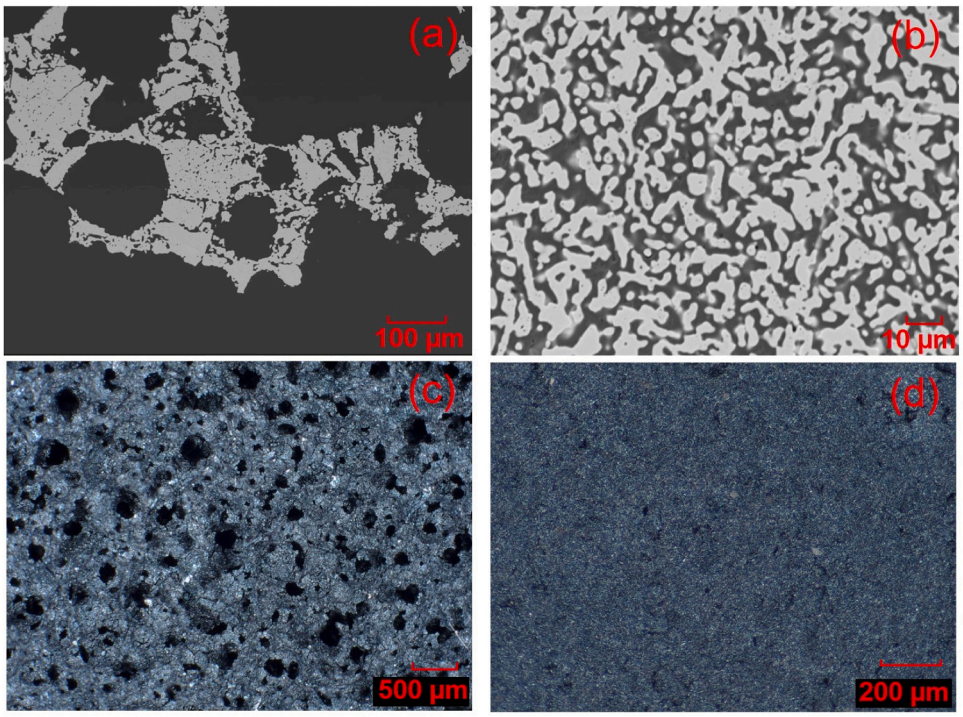

Fig. 2. Porous structure observed by a field emission electron probe microanalyzer for 100% TiO_x LP (a) and SP (b) and by a digital microscope for 100% TiO_x LP (c) and SP (d).

however, very similar chemical composition was obtained in this study. Ti_4O_7 and Ti_5O_9 are the most conductive Magnéli phases and the most suitable phases for application in the anodic oxidation process [50]. Raman spectra was performed for further confirmation of chemical composition. With a laser energy filter of 5%, the absence of well-defined peaks is typical of TiO_x phases (Fig. SI-3), while the presence of well-defined peaks at 261, 408 and 611 cm^{-1} when using high laser energy (filter set at 50%) highlighted the re-oxidation of the material to TiO_2 under high laser irradiation [40]. The chemical composition of the Ti/TiO_x electrode was already described in [40]. Data are given in SI (Fig. SI-4).

3.1.4. *Electrochemical characteristics*

Fig. 4 presents the LSV curves related to the oxygen evolution reaction when using 100% TiO_x LP and SP. 100% TiO_x LP has an oxygen evolution potential (OEP) of 2.85 V vs Ag/AgCl/3 M KCl, which is comparable to that of Ti/TiO_x foam (2.82 V vs Ag/AgCl/3 M KCl) (Table 2). A high value of OEP corresponds to the ability of electrode materials to generate large amount of $^{\bullet}OH$ that are available for reaction with organic compounds at the electrode surface [51,52]. By comparison, 100% TiO_x SP has a lower OEP of 2.29 V vs Ag/AgCl/3 M KCl. It does not necessarily mean that this material is less suitable for generation of $^{\bullet}OH$. The lower OEP obtained for 100% TiO_x SP might be ascribed to the higher EASA since it ensures more active sites for water oxidation at the anode surface [53,54]. Such behavior is beneficial for reducing the energy consumption of the process.

EASA was then obtained from CV (detailed results in SI (Fig. SI-5)). The determined EASA of 100% TiO_x LP and SP were 1096 and 7411 cm^2, corresponding to roughness factors of 46 and 416, respectively (Table 2). The EASA of 100% TiO_x SP accounted for 31% of its total surface area (SA) (calculated from the specific surface area obtained from Hg porosimetry). This lower ratio might be a consequence of a lack of interconnectivity between some pores. The 100% TiO_x LP had the lowest EASA to SA ratio (13%), which is consistent with the defects observed within the porous structure (Fig. 2(a)). The highest value was obtained for the Ti/TiO_x foam (68%). This result shows that coating of a porous structure might be a suitable strategy in terms of interconnectivity of pores.

3.2. *Reactivity of TiO_x electrodes in stirred-tank configuration*

During AO process, $^{\bullet}OH$-mediated oxidation is a key mechanism allowing the degradation and mineralization of organic compounds. Fig. 5(a) shows the degradation kinetic of TA, which is related to the reactivity of different TiO_x electrodes for $^{\bullet}OH$-mediated oxidation. Similar performance was obtained for 100% TiO_x LP and Ti/TiO_x foam, while the slowest kinetic was obtained with 100% TiO_x SP. The degradation rate constant was 2.4-times lower than that obtained with Ti/TiO_x foam and 100% TiO_x LP. A previous study showed that the porous structure of electrodes has a significant impact on the effectiveness of the process, even in stirred-tank reactor [40]. In this configuration, a thick diffusion boundary layer forms at the electrode/solution interface. Therefore, it was highlighted that coarse roughness (i.e., large pores) with characteristic scale larger than the diffusion boundary layer is actually more suitable for mass transport enhancement in stirred-tank reactor. In fact, fine roughness (i.e., small pores) is averaged within the diffusion field and does not provide additional surface for mass transport enhancement of organic compounds from the bulk to the electrode surface. The comparison of results obtained with both Ti/TiO_x foam, 100% TiO_x LP (large pore size) and 100% TiO_x SP (small pore size) confirms the advantage of the presence of a coarse roughness for mass transport enhancement in stirred-tank reactor.

Similar trends were obtained as regards to the TOC removal. Higher mineralization yields were obtained with Ti/TiO_x foam and 100% TiO_x LP, compared to 100% TiO_x SP (Fig. 5(b)). The slightly different values obtained between Ti/TiO_x foam and 100% TiO_x LP might be ascribed to the involvement of different electrocatalytic phenomena than $^{\bullet}OH$-mediated oxidation for conversion of degradation by-products to CO_2 (e.g., DET, other radical species). These mineralization yields correspond to low mineralization current efficiency for all electrodes, i.e., 6.6%, 8.2% and 4.3% for Ti/TiO_x foam, 100% TiO_x LP and 100% TiO_x SP. It was mainly ascribed to the operation of the process under strong mass

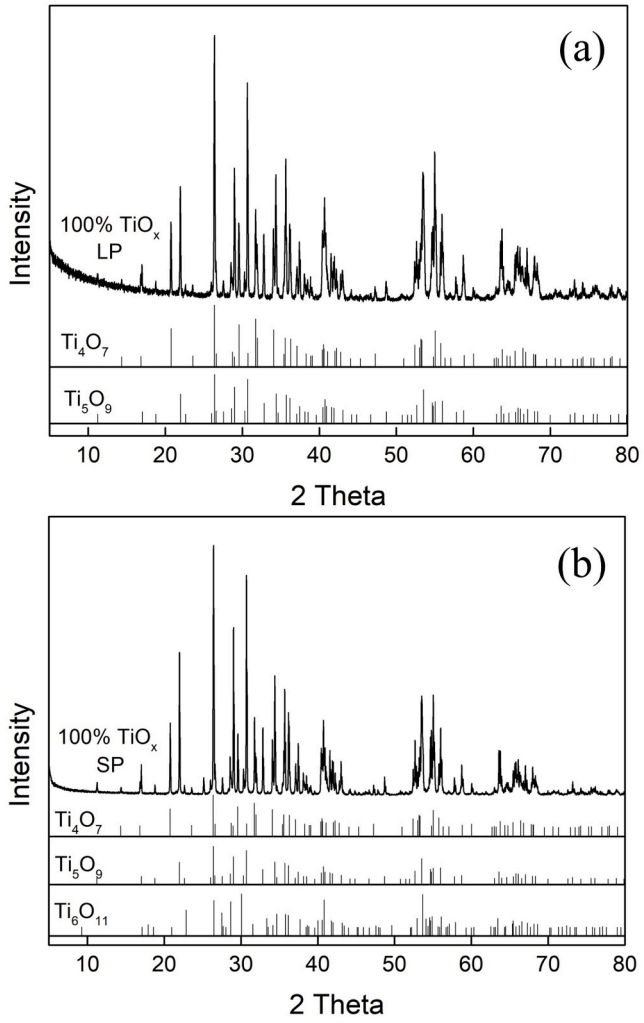

Fig. 3. XRD patterns for 100% TiO_x LP (a) and SP (b) electrodes (reference patterns: PDF2–2004).

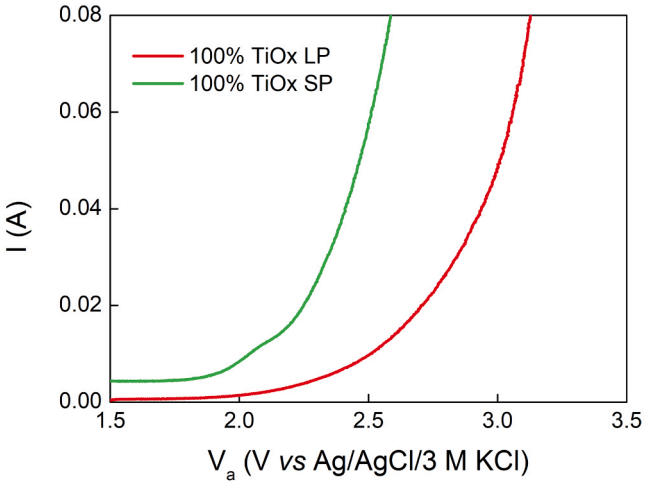

Fig. 4. LSV curves of 100% TiO_x LP and SP (reference electrode: Ag/AgCl/3 M KCl, supporting electrolyte: 100 mM $NaClO_4$, scan rate: 0.01 V s^{-1}).

transport limitation. It highlights that the stirred-tank reactor could not take full advantage of these porous materials due to the thick diffusion boundary layer at the electrode-solution interface. Therefore, the effectiveness of these porous electrodes was further investigated in terms of reactivity for DET and $^{\bullet}OH$-mediated oxidation in flow-through configuration.

Table 2
Electrochemical characteristics of TiO_x electrodes.

	OEP (V vs Ag/AgCl/ 3 M KCl)	EASA (cm^2)	EASA/ SA	Geometric surface area (cm^2)	Roughness factor
Ti/TiO_x foam	2.82*	1620	0.68	23.6	69
100% TiO_x LP	2.85	1096	0.13	23.6	46
100% TiO_x SP	2.29	7411	0.31	17.8	416

* Data obtained in similar operating conditions from Ma et al. (2022)

3.3. *Reactivity of TiO_x electrodes for direct electron transfer in flow-through configuration*

Fig. 6 shows the TOC conversion yield (a) and TOC removal rate (in term of grams of C removed per hour and per square meter of membrane) (b) of OA by different porous TiO_x electrodes in flow-through configuration, as regards to the volumetric filtration flux. Dashed lines represent the effectiveness achieved in stirred-tank reactor for specific electric charges (0.042 A h L^{-1} for 100% TiO_x LP and 0.026 A h L^{-1} for 100% TiO_x SP) similar to those applied at the optimal flux (1200 L h^{-1} m^{-2} for 100% TiO_x LP and 1940 L h^{-1} m^{-2} for 100% TiO_x SP) in flow-through reactor. The full degradation kinetics obtained in stirred-tank reactor are given in Fig. SI-6.

The mineralization yield was observed to decrease when increasing the volumetric filtration flux. This decreasing trend was ascribed to the lower residence time of OA molecules within porous electrodes. However, the TOC removal rate was improved when increasing the volumetric filtration flux owing to better mass transport conditions of OA towards the surface of electrodes.

Compared to results obtained in the stirred-tank reactor, OA degradation rate (Fig. 6(b)) was greatly enhanced for all electrodes in flow-through reactor. The optimal filtration flux was 1940 L h^{-1} m^{-2} for 100% TiO_x SP and around 1200 L h^{-1} m^{-2} for Ti/TiO_x foam and 100% TiO_x LP. At these fluxes, OA degradation rate using 100% TiO_x LP and SP was enhanced by 1.9 and 21 times, respectively. Correspondingly, mineralization current efficiency of OA increased from 2.7% and 1.8% in stirred-tank reactor to 12% and 52% in flow-through reactor for 100% TiO_x LP and 100% TiO_x SP, respectively (Fig. 7). These results highlight that the application in flow-through configuration is the key point for taking advantage of the internal porosity and EASA of porous electrodes.

Increasing the filtration flux was a key parameter for improving OA degradation rate (Fig. 8) and mineralization current efficiency. Such behavior indicates that the convection rate was the limiting phenomenon at low filtration flux. Besides, much higher enhancement of reaction rates was obtained with 100% TiO_x SP compared to Ti/TiO_x foam and 100% TiO_x LP. For example, the maximum OA mineralization rate obtained with 100% TiO_x SP was 4.0 and 4.8 times higher than the one obtained with 100% TiO_x LP and Ti/TiO_x foam, respectively. This lower efficiency might be ascribed to a limitation from diffusion within pores due to the larger pore size of Ti/TiO_x foam and 100% TiO_x LP. In fact, a limitation from pore diffusion might become significant when the time scale of diffusion (t_D, Eq. 6) exceeds the time scale of convection (t_C, Eq. 7), i.e., when the time required for target compounds to diffuse from the inside of pores to pore surface becomes longer than the residence time of target compounds within the electro-active volume of the electrode. The comparison of t_c and t_d is provided in detail in Fig. SI-7. For example, by taking into consideration the median pore radius (according to pore

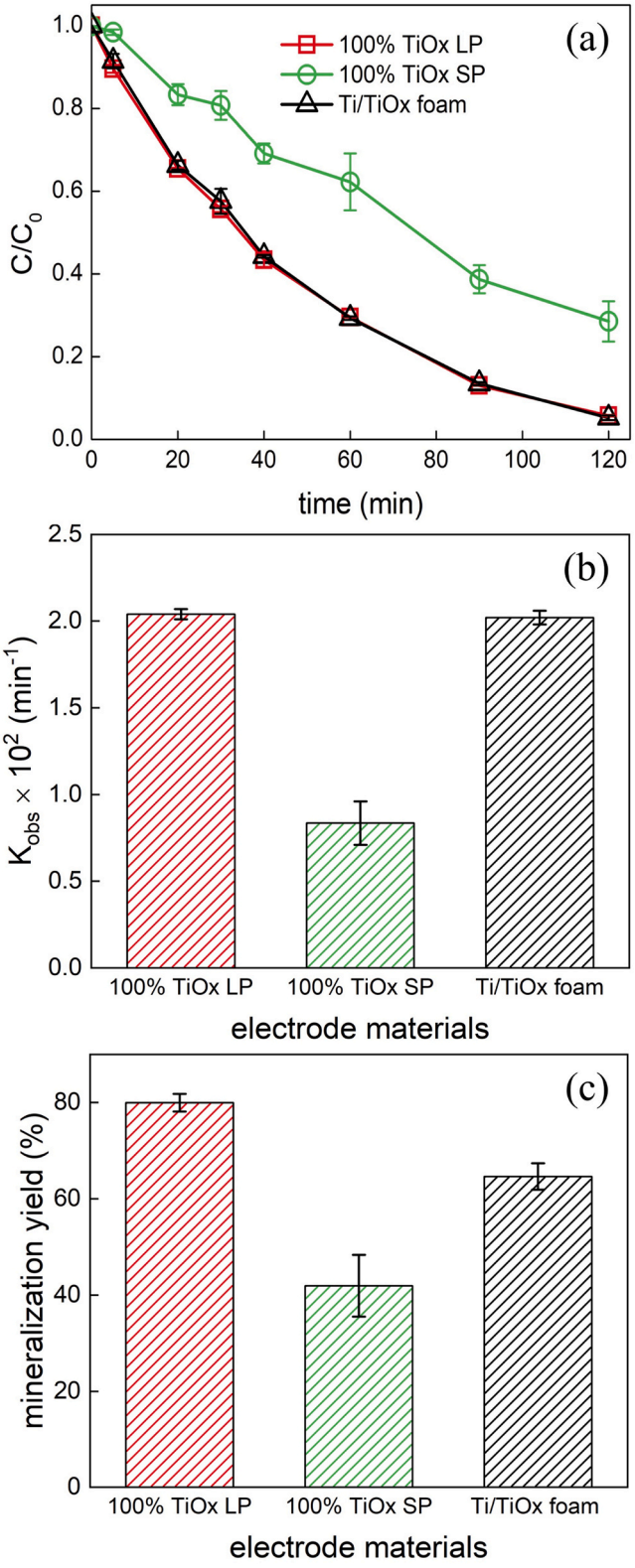

Fig. 5. Degradation kinetics of TA (a) with pseudo first order rate constants (b) during anodic oxidation and mineralization yield after 2 h of treatment (c) with 100% TiO_x anodes in stirred-tank reactor compared with Ti/TiO_x foam (initial $C_{TA} = 0.1$ mM, $S_{electrode}/V_{solution} = 7.9\ m^{-1}$, current density = 5 mA cm^{-2}).

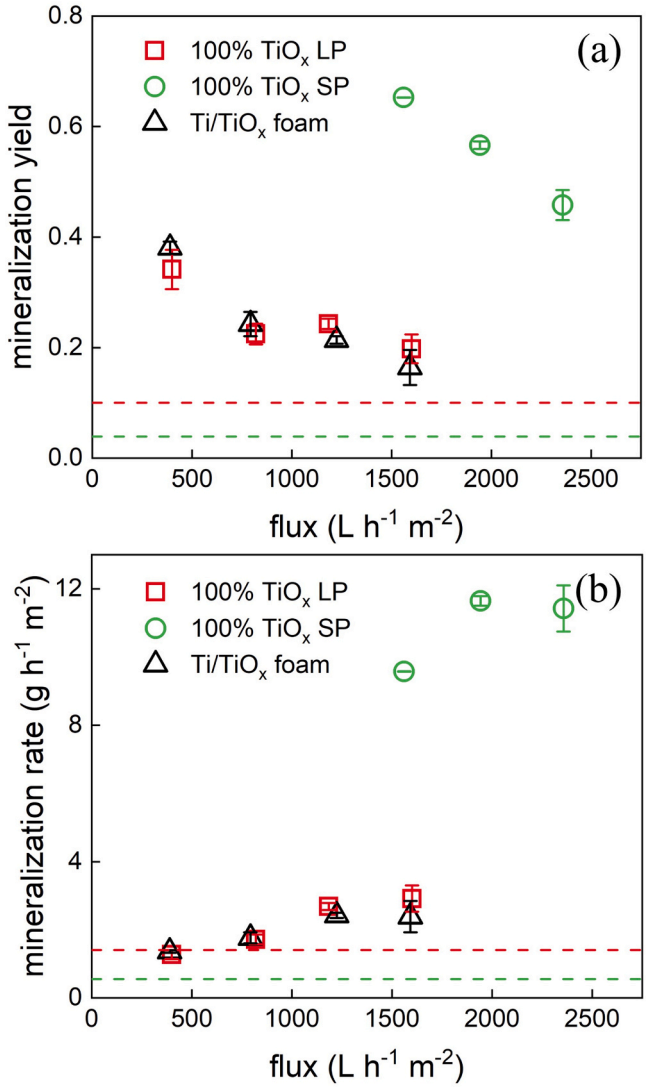

Fig. 6. OA conversion yield (regarding TOC) (a) and mineralization rate (b) by 100% TiO_x LP, SP and Ti/TiO_x foam in flow-through configuration in comparison with the results of 100% TiO_x anodes (dash lines) obtained in stirred-tank reactor with the same electric charge applied. Operating conditions: $[OA]_0 = 0.4$ mM, effective surface area $= 12.56\ cm^{-2}$, current density $= 5\ mA\ cm^{-2}$.

volume) of 100% TiO_x LP and $l = 0.2$ mm, $t_D > t_C$ would be reached at J $\approx 123\ L\ h^{-1}\ m^{-2}$ (i.e., below the range of flux tested in this study). By comparison, with the 100% TiO_x SP, the lower pore size involves that $t_D > t_C$ would be reached only at $J = 691 \times 10^3\ L\ h^{-1}\ m^{-2}$ (a value much higher than the range of operating conditions that were implemented in this study).

$$t_D = r_p^2 / D \tag{6}$$

$$t_C = l/v \tag{7}$$

where r_p is the average pore radius (m), D is the diffusion coefficient of the target compounds ($m^2\ s^{-1}$) ($1.0 \times 10^{-9}\ m^2\ s^{-1}$ for oxalic acid (Šljukić et al., 2007)), l is the electro-active layer thickness (m) and v is the average pore velocity ($m\ s^{-1}$).

These results highlight that using electrodes with large pore size for the treatment of low concentration of organic compounds might still result in a strong mass transport limitation related to the radial diffusion within pores, even in flow-through configuration. On the contrary, when

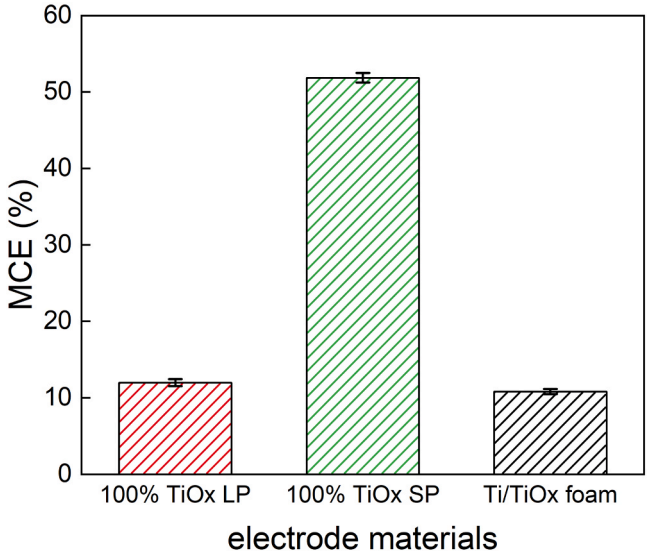

Fig. 7. Mineralization current efficiency of 0.4 mM OA by TiO_x anodes at optimal flux (1943 L h^{-1} m^{-2} for 100% TiO_x SP, 1185 L h^{-1} m^{-2} for 100% TiO_x LP and 1224 L h^{-1} m^{-2} for Ti/TiO_x foam) (effective surface area = 12.56 cm^{-2}, current density = 5 mA cm^{-2}).

using 100% TiO_x SP with low pore size, the mass transport rate was easily improved by increasing the volumetric filtration flux (without significant limitation from pore diffusion). At the highest volumetric filtration flux, the plateau of effectiveness might then be related to the kinetic limitation related to the electrocatalytic phenomenon.

These results are important for determining the application range of these different electrode materials. By assuming that 100% TiO_x SP is limited by pore diffusion, it is possible to consider that mass transport of target pollutant to the electrode surface is controlled by the pore diffusion rate constant (k_d), which can be calculated as follow [35]:

$$k_d = D/r \tag{8}$$

Where, D is the diffusion coefficient (1×10^{-9} m^2 s^{-1} for OA) [55]. For 100% TiO_x LP, it corresponds to a value of 1.6×10^{-5} m s^{-1}. From this value, it is possible to estimate a corresponding limiting current density (j_{lim}) for the removal of chemical oxygen demand (*COD*, corresponding to the amount of organic compounds in solution) as:

$$j_{lim} = 4\,F\,k\,COD \tag{9}$$

Where, F is the Faraday constant and k the mass transport rate constant (k_d in this case). For example, for COD = 30 mg L^{-1}, the value of j_{lim} would be only 0.58 mA cm^{-2}. Such low value of j_{lim} would lead to either low Faraday efficiency (when applying higher current density) or very low productivity of the process (when applying a small current close to this value of j_{lim}). However, higher value of j_{lim} would be reached for the treatment of medium concentration target pollutants (e.g., j_{lim} = 5.0 mA cm^{-2} for COD = 260 mg L^{-1}). For comparison, when mass transport is controlled by convection (i.e., by the volumetric filtration flux) with 100% TiO_x SP, higher values of mass transport rate constant can be reached. For example, for a convection rate constant of $k_c = 1.4 \times 10^{-4}$ m s^{-1} (corresponding to a flux of 500 L h^{-1} m^{-2}), the corresponding limiting current density would be 5.0 mA cm^{-2} for the treatment of a small concentration of COD of 30 mg L^{-1} (in case of absence of kinetic limitation).

3.4. Reactivity of TiO_x electrodes for $^{\bullet}OH$-mediated oxidation in flow-through configuration

For $^{\bullet}OH$-mediated oxidation, the TA degradation rates obtained with

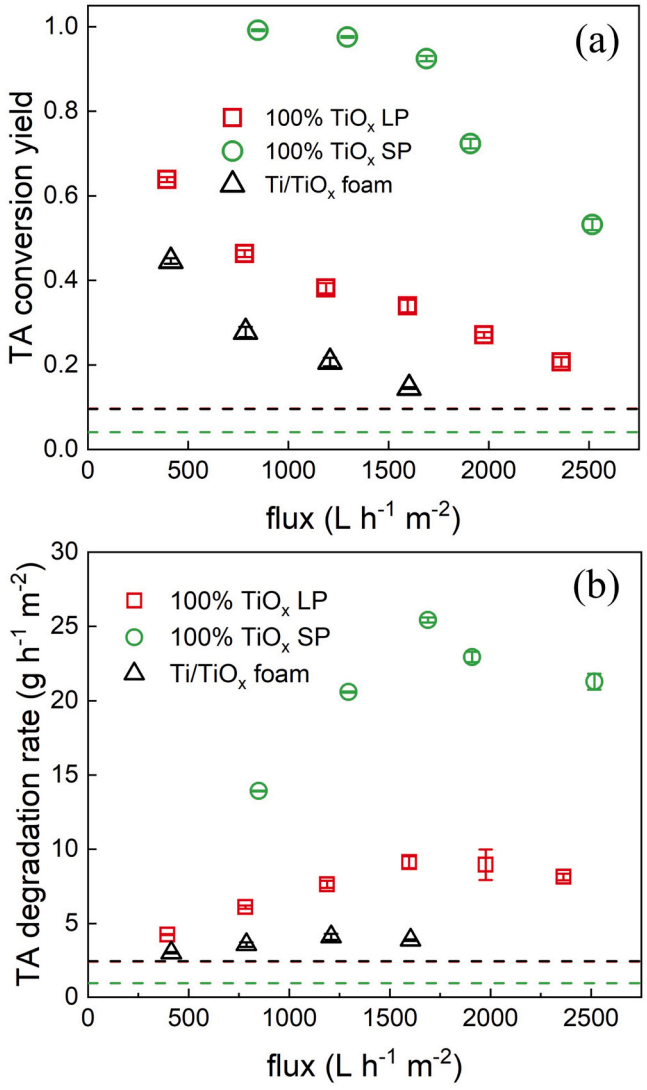

Fig. 8. TA conversion yield (a) and degradation rate (b) during anodic oxidation in flow-through reactor compared to the application in stirred-tank reactor (dashed lines) by 100% TiO_x LP, SP and Ti/TiO_x foam. Operating conditions: $[OA]_0$ = 0.1 mM, effective surface area = 12.56 cm^{-2}, current density = 5 mA cm^{-2}.

100% TiO_x LP, 100% TiO_x SP and Ti/TiO_x foam followed similar trends compared to OA. The TA conversion (degradation) yields decreased with increasing the filtration flux, but the degradation rates (in terms of grams of TA degraded per hour and per square meter of electrode) were improved when increasing the filtration flux (Fig. 8).

Firstly, at the optimum flux, TA degradation rates in the flow-through reactor were enhanced by 3.8, 1.7, and 27 times compared to the stirred-tank reactor (dashed lines) for 100% TiO_x LP, Ti/TiO_x foam and 100% TiO_x SP, respectively. The most significant enhancement of TA reaction rate was obtained with 100% TiO_x SP. The maximum TA degradation rate obtained with 100% TiO_x SP was 2.8 and 6.2 times higher than with 100% TiO_x LP and Ti/TiO_x foam, respectively. As detailed previously for OA reaction rate, it might be mainly ascribed to the absence of any limitation from pore diffusion in this range of filtration flux, while the larger pores of Ti/TiO_x foam and 100% TiO_x LP involved a significant limitation from diffusion within pores. Fig. 9 shows that MCE for TA was also strongly enhanced in flow-through configuration compared to stirred-tank reactor. The MCE was close to 100% at the optimum flux for 100% TiO_x, which highlights good mass transport conditions for the treatment of 0.1 mM of TA. Lower MCE

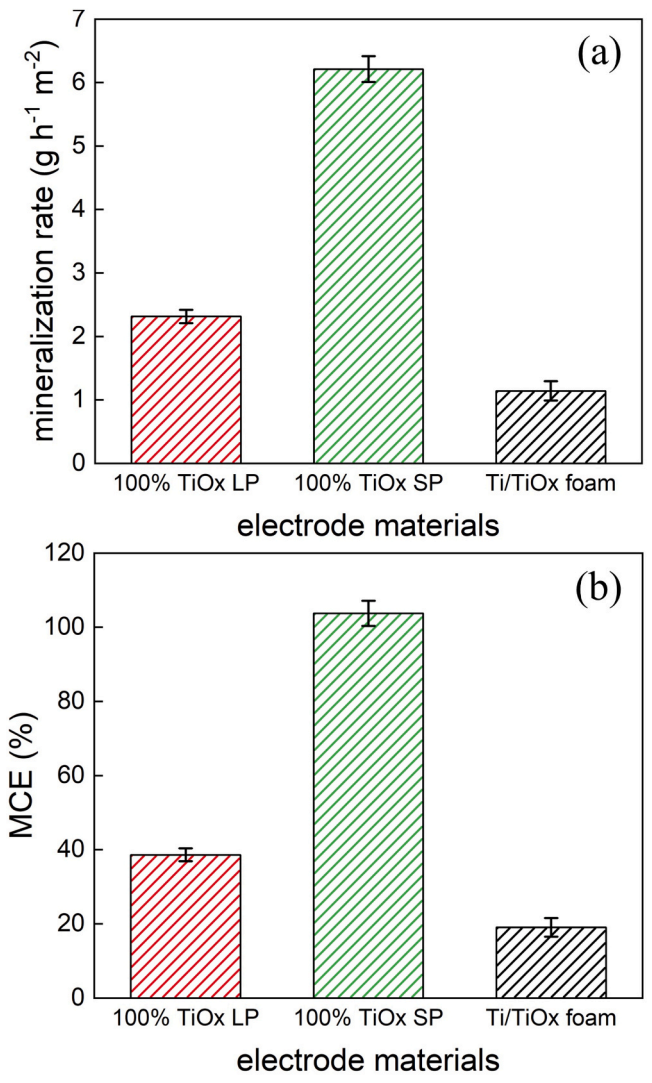

Fig. 9. TA mineralization rate (in terms of TOC) (a) and mineralization current efficiency (b) by 100% TiO_x LP (1190 L h^{-1} m^{-2}), SP (1910 L h^{-1} m^{-2}) and Ti/TiO_x foam (1210 L h^{-1} m^{-2}) during anodic oxidation in flow-through configuration (initial C_{TA} = 0.1 mM, effective surface area = 12.56 cm^{-2}, current density = 5 mA cm^{-2}).

values were obtained for both Ti/TiO_x foam and 100% TiO_x LP because of this mass transport limitation that promotes waste reactions (e.g. •OH dimerization).

Overall, the values of MCE were higher for experiments with TA compared to OA. Data obtained from LSV with OA did not show any oxidation peak below the OEP that may be attributed to OA oxidation (Fig. SI-8), thus indicating that oxidation of OA at TiO_x electrode required high anodic potential (in the region of water oxidation). Besides, OA has low reaction rates with •OH. Therefore, a portion of the current was wasted for •OH formation and further evolution to O_2 in the case of OA oxidation. On the contrary, TA was also able to react with •OH with high reaction rate, thus resulting in higher MCE.

The reactivity of TiO_x membranes for •OH-mediated oxidation has been investigated in previous studies (Table 3). The TA degradation efficiency at optimum condition obtained in this study (25.4 g h^{-1} m^{-2} with 100% TiO_x SP) is higher than the results obtained by Guo et al. (2016) [35] (1.1 g h^{-1} m^{-2}) and Nayak and Chaplin (2018) [41] (5.3 g h^{-1} m^{-2}) using porous Ti_4O_7 electrodes. Only Gayen et al. (2018) [56] reported a higher value (72.1 g h^{-1} m^{-2}). However, it is difficult to compare these results since crucial operating conditions (e.g., initial TA concentration and applied current density / anodic potential) were different. The energy consumption per log removal of target molecules is a more suitable parameter since it takes into consideration both current / cell potential and process effectiveness. However, it does not take into consideration the variability of the feed effluent (nature of pollutant, concentration, electrolyte composition). Based on this parameter, the energy requirement in this flow-through reactor (0.26 kWh m^{-3}) was 37 times lower compared to the stirred-tank reactor (9.6 kWh m^{-3}) and the results obtained in this study were comparable with the results obtained by Gayen et al. (2018) [56].

It is interesting to notice that TA degradation rate with Ti/TiO_x foam was significantly lower compared to 100% TiO_x LP (Fig. 8), while similar results were previously obtained for OA degradation rate (Fig. 6). These results might be ascribed to the specific structure of the Ti/TiO_x foam, for which only the top of the electrode was coated. While both Ti substrate and TiO_x coating could participate in the removal of OA through DET, only the TiO_x coating was able to generate physisorbed •OH and allowed for contributing to •OH-mediated oxidation. Thus, the electro-active thickness for •OH formation might not reach a value above ≈ 100 μm, according to images obtained from scanning electron microscopy [40] (Fig. SI-2). Therefore, the time scale for convection (Eq. 7) within this smaller electro-active thickness was reduced. Such phenomenon might result in further mass transfer limitation and lower reaction rate for •OH-mediated oxidation.

Table 3
Comparison of the performances with previous studies in terms of electrode reactivity for DET (OA removal) and •OH-mediated oxidation (TA removal).

Predominant TiO_x phase	Pore size (μm)	Working mode	Probe molecule ($C_{initial}$, mM)	V_{anodic} (V vs SHE) or j (mA cm^{-2})	Flux (L h^{-1} m^{-2})	Conversion yield	Degradation rate (g h^{-1} m^{-2})	Mineralization yield	Mineralization rate (g h^{-1} m^{-2})	E_{EO} (kWh m^{-3})	Ref
Ti_4O_7	2.99 (median)	Flow-through	OA (1)	V_a = 2.94	793	0.51	36.1	0.51	9.6 (TOC)	—	[35]
			TA (0.1)	V_a = 2.64	116	0.58	1.1	—	—	—	
Ti_4O_7	1.4 (median)	Flow-through	OA (1)	V_a = 3.16	656	0.98	53.3	0.98	14.2 (TOC)	—	[41]
			TA (0.1)	V_a = 2.86		0.49	5.3	—	1.9 (COD)	—	
Ti_4O_7	0.41	Flow-through	TA (1)	V_a = 3.50	600	0.72	72.1	0.65	37.4 (COD)	4.4	[56]
Ti_4O_7 / Bi-doped SnO_2	0.36					0.99	98.6	0.97	55.9 (COD)	< 0.5	
Ti_4O_7, Ti_5O_9	2.2 (median)	Flow-through	OA (0.4)	j = 5	1943	0.56	43.7	0.56	11.6 (TOC)	0.36	This study (100% TiO_x SP)
		Stirred-tank	TA (0.1)		1909	0.72	22.9	0.34	6.2 (TOC)	0.26	
			OA (0.4)		t = 5 min	0.04	2.1	0.04	0.6	10	
			TA (0.1)		V = 300 mL	0.04	1.0	—	—	9.6	

A slight decrease of TA reaction rate was obtained for all electrode materials at high filtration flux. First, reaching a plateau might be related to the kinetic limitation for •OH-mediated oxidation of TA that might occur at the highest filtration fluxes (i.e., when the residence time within the electro-active volume decreases). In addition, high flux helped sweeping O_2 gas bubbles from the electrode surface and therefore promoted competitive reaction of 2 e^- oxidation of water to O_2, which may reduce the generation of •OH from 1 e^- oxidation of water [35,38,41,56].

3.5. Is it possible to obtain a quantitative correlation between the porous structure of the electrode and the effectiveness of the process?

A recent theoretical work on solute transport and reaction in porous electrodes has highlighted that conversion values obtained with different kinds of porous materials might be correlated with the product $Da\ S_s\ L$, where Da is the Damköhler number (Eq. 8), S_s is the specific surface area (in $m^2\ m^{-3}$) and L is the thickness of the reactive zone [57]. The term $S_s\ L$ was identified as an aspect ratio of the porous structure of the material, which plays a crucial role in process effectiveness. Results from numerical simulations emphasized that conversion values collapsed on a single master curve when it was plotted as a function of this product $Da\ S_s\ L$ [57].

$$Da = k_r/u \tag{10}$$

where k_r is the rate constant for oxidation of the target compound (m s^{-1}) and u is the fluid velocity (m s^{-1}).

This approach was applied to experimental results obtained in this study. A lower limit (lower bound) of the surface area normalized k_r was estimated from the conversion rate obtained with 100% TiO_x SP at the optimal flux since the kinetic limit for oxidation of target compounds at TiO_x surface was approached in these conditions (4.3×10^{-4} m s^{-1} and 3.1×10^{-4} m s^{-1} for TA and OA, respectively). Then, the specific surface area was calculated from EASA and material porosity. The value of L for TA degradation using Ti/TiO_x foam was set at an upper limit of 0.1 mm as only the top of the Ti substrate was coated with a TiO_x layer allowing the formation of •OH. Then, all the other values of L were fitted for collapsing all experimental data points on a single master curve for TA degradation (Fig. 10 (a)) and OA degradation (Fig. 10 (b)).

Overall, high values of the product Da S_s L were obtained. The calibrated values of L were 0.16 and 0.4 mm for 100% TiO_x SP and 100% TiO_x LP for both TA and OA conversion experiments. The value of L (thickness of the reactive zone) might depend on several parameters including pore size, interconnection of pores, material conductivity and anodic potential required for conversion of the target compound. As observed from LSV data (Fig. SI-8), both TA and OA oxidation occur at high anodic potential (in the region of water oxidation), which might explain the similar value of L obtained in both cases. The L value obtained for the Ti/TiO_x foam increased from 0.1 mm (for TA experiments) to 0.2 mm for OA degradation, which might be ascribed to the participation of the Ti substrate to the removal of OA through DET. These values of L are interesting for comparing the different electrode materials. However, these values have to be taken cautiously since further investigations would be required for precise determination of the thickness of the reactive zone.

Based on this approach, a good correlation was obtained between experimental values of conversion of both TA and OA and the value of the product $Da\ S_s\ L$. In this range of operating conditions, a linear correlation was obtained (with $R^2 = 0.96$ and 0.97 for TA and OA experiments, respectively) (Fig. 10). Similar slope was obtained for both TA and OA experiments, thus indicating the robustness of the approach. A correlation under the form of $y = (1 - \exp(-ax))$ might be also suitable for taking into consideration the capping of conversion values to 1 for high values of $Da\ S_s\ L$ (Fig. SI-9) [57]. Such kind of correlation is crucial for helping to design novel electrode materials with suitable porous structure. An ideal design of anode material should be able to optimize (i) the value of k_r through a suitable chemical composition (for increasing Da value) and (ii) the value of the product $S_s\ L$ through a suitable porous structure (low pore size for improving S_s and high conductivity / good interconnection of pores for improving L). Material design should also take into consideration the intended application, particularly in terms of concentration of target compounds, presence of fouling components, and pressure drop during filtration. More specifically, further decreasing material pore size could contribute to fouling issues and increase operating costs due to pressure drop during filtration at high volumetric fluxes.

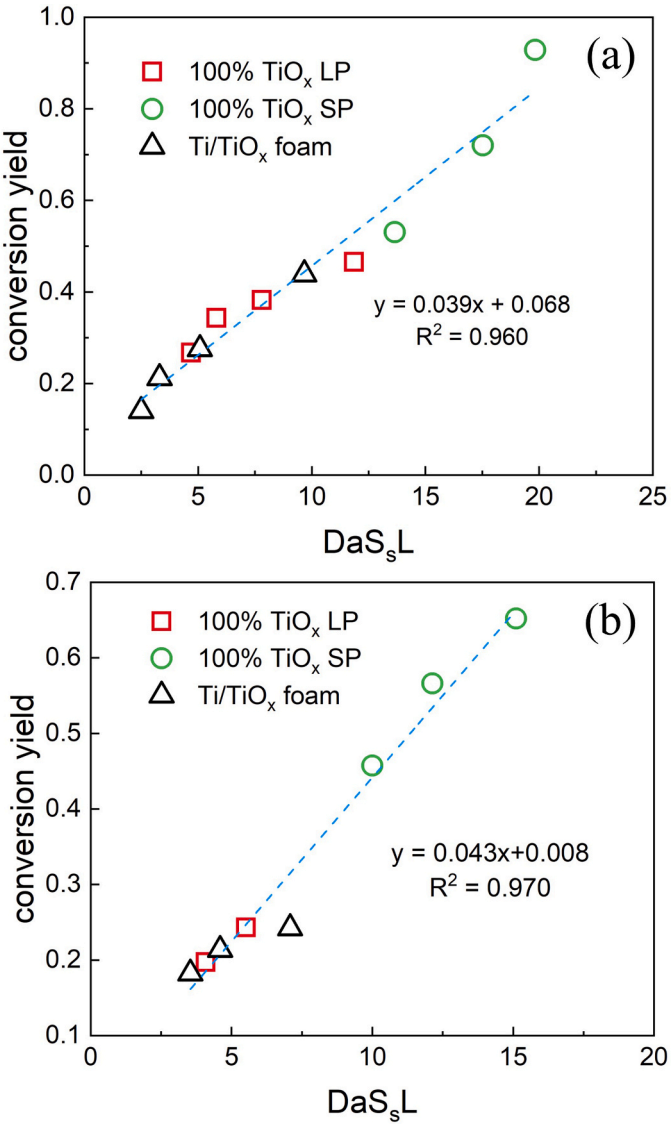

Fig. 10. Plot of conversion yield vs DaSsL for TA degradation (a) and OA mineralization (b) by TiO_x anodes in flow-through reactor and the results of linear fitting.

4. Conclusions

Both 100% TiO_x electrodes presented very similar chemical composition, including Ti_4O_7 and Ti_5O_9 as main phases. However, their very different pore size distribution highlighted the role of the porous structure of these materials in the electrooxidation process.

In stirred-tank reactor, coarse roughness (i.e., large pores) was more favorable for improving mass transport conditions since fine roughness (small pores) was averaged within the diffusion field.

In flow-through reactor, convection through the porous electrode allowed for taking advantage of the internal EASA, while diffusion limitation is avoided from fast radial diffusion within small pores. For example, TA degradation rate was multiplied by 27 times when using 100% TiO_x SP (small pore size, ≈ 2.2 μm) under optimal volumetric filtration flux compared to the reaction rate obtained in stirred-tank reactor. When using electrodes with larger pore size (Ti/TiO_x foam and 100% TiO_x LP, ≈ 100 μm), the limitation from pore diffusion was still significant and lowered the effectiveness. The time scale for diffusion was higher than the time scale for convection, even at low filtration flux. This limitation was further enhanced when using a Ti/TiO_x foam for TA oxidation since the residence time within the reactive zone for $^{\bullet}OH$-mediated oxidation was reduced to the superficial TiO_x-coated layer of the electrode. Such diffusion limitation did not occur when using 100% TiO_x SP due to smaller pore size. However, the degradation rate of target compounds reached a plateau and slightly decreased for fluxes higher than 1600 L h^{-1} m^{-2} because (i) the kinetic limitation was approached (ii) high filtration flux enhanced competition with the OER.

Finally, conversion values of OA and TA in flow-through configuration using the different electrode materials were correlated with values of the product $Da\ S_s\ L$. A single master curve was obtained. Such approach might be helpful for the design of novel electrode materials with suitable porous structure.

These results highlight advantages and drawbacks related to the different porous structure of electrodes and emphasize the key role of the reactor configuration. Electrodes with low pore size are the most suitable to apply in flow-through configurations for mass transport enhancement and efficient removal of low concentration of organic pollutants. However, electrodes with large pore size might still provide a solution for avoiding high-pressure drop and fouling issues, particularly for the treatment of medium concentrations (i.e., lower limitation from mass transport).

CRediT authorship contribution statement

Jing MA: Investigation, Methodology; Data curation; Formal analysis Writing- Original draft preparation, Reviewing and Editing. **Clement TRELLU:** Conceptualization, Supervision, Validation, Formal analysis, Reviewing and Editing. **Nihal OTURAN:** Supervision, Formal analysis, Methodology, Visualization, Validation. **Stephan RAFFY:** Funding acquisition, Investigation, Methodology. **Mehmet A. OTURAN:** Supervision, Conceptualization, Funding acquisition, Reviewing and Editing.

Declaration of Competing Interest

The authors declare that they have no known competing financial interests or personal relationships that could have appeared to influence the work reported in this paper.

Data availability

Data will be made available on request.

Acknowledgements

Jing Ma acknowledges China Scholarship Council for the financial support for her PhD work (201906970041). Authors acknowledge Saint-Gobain Research Provence for providing TiO_x electrodes. Authors acknowledge Chloé Fourdrin for Raman spectroscopy analyses.

Appendix A. Supporting information

Supplementary data associated with this article can be found in the online version at doi:10.1016/j.apcatb.2023.123472.

References

[1] M. Panizza, G. Cerisola, Direct And Mediated Anodic Oxidation of Organic Pollutants, Chem. Rev. 109 (2009) 6541–6569, https://doi.org/10.1021/cr9001319.
[2] Z. Hu, J. Cai, G. Song, Y. Tian, M. Zhou, Anodic oxidation of organic pollutants: Anode fabrication, process hybrid and environmental applications, Curr. Opin. Electrochem. 26 (2021), 100659, https://doi.org/10.1016/j.coelec.2020.100659.
[3] J. Radjenovic, D.L. Sedlak, Challenges and Opportunities for Electrochemical Processes as Next-Generation Technologies for the Treatment of Contaminated Water, Environ. Sci. Technol. 49 (2015) 11292–11302, https://doi.org/10.1021/acs.est.5b02414.
[4] B.P. Chaplin, Critical review of electrochemical advanced oxidation processes for water treatment applications, Env. Sci. Process. Impacts 16 (2014) 1182–1203, https://doi.org/10.1039/C3EM00679D.
[5] I. Sirés, E. Brillas, M.A. Oturan, M.A. Rodrigo, M. Panizza, Electrochemical advanced oxidation processes: today and tomorrow. A review, Environ. Sci. Pollut. Res. 21 (2014) 8336–8367, https://doi.org/10.1007/s11356-014-2783-1.
[6] M.A. Oturan, Outstanding performances of the BDD film anode in electro-Fenton process: Applications and comparative performance, Curr. Opin. Solid State Mater. Sci. 25 (2021), 100925, https://doi.org/10.1016/j.cossms.2021.100925.
[7] R. Montenegro-Ayo, T. Pérez, M.R.V. Lanza, E. Brillas, S. Garcia-Segura, A.J. Dos Santos, New electrochemical reactor design for emergent pollutants removal by electrochemical oxidation, Electrochim. Acta 458 (2023), 142551, https://doi.org/10.1016/j.electacta.2023.142551.
[8] S. Garcia-Segura, X. Qu, P.J.J. Alvarez, B.P. Chaplin, W. Chen, J.C. Crittenden, Y. Feng, G. Gao, Z. He, C.-H. Hou, X. Hu, G. Jiang, J.-H. Kim, J. Li, Q. Li, J. Ma, J. Ma, A.B. Nienhauser, J. Niu, B. Pan, X. Quan, F. Ronzani, D. Villagran, T. D. Waite, W.S. Walker, C. Wang, M.S. Wong, P. Westerhoff, Opportunities for nanotechnology to enhance electrochemical treatment of pollutants in potable water and industrial wastewater – a perspective, Environ. Sci. Nano. 7 (2020) 2178–2194, https://doi.org/10.1039/D0EN00194E.
[9] E. Brillas, C.A. Martínez-Huitle, Decontamination of wastewaters containing synthetic organic dyes by electrochemical methods. An updated review, Appl. Catal. B Environ. 166–167 (2015) 603–643, https://doi.org/10.1016/j.apcatb.2014.11.016.
[10] X. Li, D. Pletcher, F.C. Walsh, Electrodeposited lead dioxide coatings, Chem. Soc. Rev. 40 (2011) 3879, https://doi.org/10.1039/c0cs00213e.
[11] B. Marselli, J. Garcia-Gomez, P.-A. Michaud, M.A. Rodrigo, Ch Comninellis, Electrogeneration of Hydroxyl Radicals on Boron-Doped Diamond Electrodes, J. Electrochem. Soc. 150 (2003) D79, https://doi.org/10.1149/1.1553790.
[12] C.A. Martínez-Huitle, S. Ferro, Electrochemical oxidation of organic pollutants for the wastewater treatment: direct and indirect processes, Chem. Soc. Rev. 35 (2006) 1324–1340, https://doi.org/10.1039/B517632H.
[13] P.V. Nidheesh, M. Zhou, M.A. Oturan, An overview on the removal of synthetic dyes from water by electrochemical advanced oxidation processes, Chemosphere 197 (2018) 210–227, https://doi.org/10.1016/j.chemosphere.2017.12.195.
[14] N. Oturan, J. Bo, C. Trellu, M.A. Oturan, Comparative Performance of Ten Electrodes in Electro-Fenton Process for Removal of Organic Pollutants from Water, ChemElectroChem 8 (2021) 3294–3303, https://doi.org/10.1002/celc.202100588.
[15] M. Rueffer, D. Bejan, N.J. Bunce, Graphite: An active or an inactive anode? Electrochim. Acta 56 (2011) 2246–2253, https://doi.org/10.1016/j.electacta.2010.11.071.
[16] F. Sopaj, N. Oturan, J. Pinson, F. Podvorica, M.A. Oturan, Effect of the anode materials on the efficiency of the electro-Fenton process for the mineralization of the antibiotic sulfamethazine, Appl. Catal. B Environ. 199 (2016) 331–341, https://doi.org/10.1016/j.apcatb.2016.06.035.
[17] R. Stirling, W.S. Walker, P. Westerhoff, S. Garcia-Segura, Techno-economic analysis to identify key innovations required for electrochemical oxidation as point-of-use treatment systems, Electrochim. Acta 338 (2020), 135874, https://doi.org/10.1016/j.electacta.2020.135874.
[18] H.J. Liu, M.Q. Luo, L.X. Yang, C.L. Zeng, C. Fu, A high strength and conductivity bulk Magnéli phase Ti_4O_7 with superior electrochemical performance, Ceram. Int. 48 (2022) 25538–25546, https://doi.org/10.1016/j.ceramint.2022.05.233.
[19] S. Liang, H. Lin, X. Yan, Q. Huang, Electro-oxidation of tetracycline by a Magnéli phase Ti_4O_7 porous anode: Kinetics, products, and toxicity, Chem. Eng. J. 332 (2018) 628–636, https://doi.org/10.1016/j.cej.2017.09.109.
[20] A.C.M. Padilha, J.M. Osorio-Guillén, A.R. Rocha, G.M. Dalpian, Ti_nO_{2n-1} Magnéli phases studied using density functional theory, Phys. Rev. B. 90 (2014), 035213, https://doi.org/10.1103/PhysRevB.90.035213.
[21] N. Aust, A. Kirste, Paired Electrosynthesis, in: G. Kreysa, K. Ota, R.F. Savinell (Eds.), Encycl. Appl. Electrochem., Springer, New York, New York, NY, 2014, pp. 1505–1510, https://doi.org/10.1007/978-1-4419-6996-5_370.
[22] S.O. Ganiyu, N. Oturan, S. Raffy, M. Cretin, R. Esmilaire, E. van Hullebusch, G. Esposito, M.A. Oturan, Sub-stoichiometric titanium oxide (Ti_4O_7) as a suitable ceramic anode for electrooxidation of organic pollutants: A case study of kinetics, mineralization and toxicity assessment of amoxicillin, Water Res 106 (2016) 171–182, https://doi.org/10.1016/j.watres.2016.09.056.
[23] H. Lin, J. Niu, S. Liang, C. Wang, Y. Wang, F. Jin, Q. Luo, Q. Huang, Development of macroporous Magnéli phase Ti_4O_7 ceramic materials: As an efficient anode for mineralization of poly- and perfluoroalkyl substances, Chem. Eng. J. 354 (2018) 1058–1067, https://doi.org/10.1016/j.cej.2018.07.210.
[24] L. Wang, M. Nickelsen, S.-Y. (Dora Chiang, S. Woodard, Y. Wang, S. Liang, R. Mora, R. Fontanez, H. Anderson, Q. Huang, Treatment of perfluoroalkyl acids in concentrated wastes from regeneration of spent ion exchange resin by

electrochemical oxidation using Magnéli phase Ti_4O_7 anode, Chem. Eng. J. Adv. 5 (2021), 100078, https://doi.org/10.1016/j.ceja.2020.100078.
[25] S. You, B. Liu, Y. Gao, Y. Wang, C.Y. Tang, Y. Huang, N. Ren, Monolithic Porous Magnéli-phase Ti_4O_7 for Electro-oxidation Treatment of Industrial Wastewater, Electrochim. Acta 214 (2016) 326–335, https://doi.org/10.1016/j.electacta.2016.08.037.
[26] B. Villanueva Martinez, H. Odier, C. Coetsier, K. Groenen Serrano, Recent advances in sub-stoichiometric TiO_2 as reactive electrochemical membranes (REM) for bio-refractory pollutants removal: A critical review, J. Environ. Chem. Eng. 11 (2023), 110203, https://doi.org/10.1016/j.jece.2023.110203.
[27] J. Xie, J. Ma, S. Zhao, T.D. Waite, Flow anodic oxidation: Towards high-efficiency removal of aqueous contaminants by adsorbed hydroxyl radicals at 1.5 V vs SHE, Water Res 200 (2021), 117259, https://doi.org/10.1016/j.watres.2021.117259.
[28] C. Li, J. Zhu, Z. Zhao, J. Wang, Q. Yang, H. Sun, B. Jiang, An efficient and robust flow-through electrochemical Ti_4O_7 membrane system for simultaneous Cr(VI) reduction and Cr immobilization with membrane cleaning by a periodic polarity reversal strategy, Sep. Purif. Technol. 297 (2022), 121424, https://doi.org/10.1016/j.seppur.2022.121424.
[29] R.M. Reis, J.A.F. Baio, F.L. Migliorini, R. da S. Rocha, M.R. Baldan, N.G. Ferreira, M.R. de V. Lanza, Degradation of dipyrone in an electrochemical flow-by reactor using anodes of boron-doped diamond (BDD) supported on titanium, J. Electroanal. Chem. 690 (2013) 89–95, https://doi.org/10.1016/j.jelechem.2012.12.003.
[30] N. Wachter, J.M. Aquino, M. Denadai, J.C. Barreiro, A.J. Silva, Q.B. Cass, N. Bocchi, R.C. Rocha-Filho, Electrochemical degradation of the antibiotic ciprofloxacin in a flow reactor using distinct BDD anodes: Reaction kinetics, identification and toxicity of the degradation products, Chemosphere 234 (2019) 461–470, https://doi.org/10.1016/j.chemosphere.2019.06.053.
[31] A. Urtiaga, P. Fernandez-Castro, P. Gómez, I. Ortiz, Remediation of wastewaters containing tetrahydrofuran. Study of the electrochemical mineralization on BDD electrodes, Chem. Eng. J. 239 (2014) 341–350, https://doi.org/10.1016/j.cej.2013.11.028.
[32] F.F. Rivera, C.P. De León, J.L. Nava, F.C. Walsh, The filter-press FM01-LC laboratory flow reactor and its applications, Electrochim. Acta 163 (2015) 338–354, https://doi.org/10.1016/j.electacta.2015.02.179.
[33] M. Chen, C. Wang, X. Zhao, Y. Wang, W. Zhang, Z. Chen, X. Meng, J. Luo, J. Crittenden, Development of a highly efficient electrochemical flow-through anode based on inner in-site enhanced TiO2-nanotubes array, Environ. Int. 140 (2020), 105813, https://doi.org/10.1016/j.envint.2020.105813.
[34] C. Trellu, B.P. Chaplin, C. Coetsier, R. Esmilaire, S. Cerneaux, C. Causserand, M. Cretin, Electro-oxidation of organic pollutants by reactive electrochemical membranes, Chemosphere 208 (2018) 159–175, https://doi.org/10.1016/j.chemosphere.2018.05.026.
[35] L. Guo, Y. Jing, B.P. Chaplin, Development and Characterization of Ultrafiltration TiO_2 Magnéli Phase Reactive Electrochemical Membranes, Environ. Sci. Technol. 50 (2016) 1428–1436, https://doi.org/10.1021/acs.est.5b04366.
[36] L. Baptista-Pires, G.-F. Norra, J. Radjenovic, Graphene-based sponges for electrochemical degradation of persistent organic contaminants, Water Res 203 (2021), 117492, https://doi.org/10.1016/j.watres.2021.117492.
[37] W. Li, R. Xiao, H. Lin, K. Yang, W. Li, K. He, L.-H. Yang, M. Pu, M. Li, S. Lv, Electro-activation of peroxymonosulfate by a graphene oxide/iron oxide nanoparticle-doped Ti_4O_7 ceramic membrane: mechanism of singlet oxygen generation in the removal of 1,4-dioxane, J. Hazard. Mater. 424 (2022), 127342, https://doi.org/10.1016/j.jhazmat.2021.127342.
[38] C. Trellu, C. Coetsier, J.-C. Rouch, R. Esmilaire, M. Rivallin, M. Cretin, C. Causserand, Mineralization of organic pollutants by anodic oxidation using reactive electrochemical membrane synthesized from carbothermal reduction of TiO_2, Water Res 131 (2018) 310–319, https://doi.org/10.1016/j.watres.2017.12.070.
[39] X. Du, M.A. Oturan, M. Zhou, N. Belkessa, P. Su, J. Cai, C. Trellu, E. Mousset, Nanostructured electrodes for electrocatalytic advanced oxidation processes: From materials preparation to mechanisms understanding and wastewater treatment applications, Appl. Catal. B Environ. 296 (2021), 120332, https://doi.org/10.1016/j.apcatb.2021.120332.
[40] J. Ma, C. Trellu, N. Oturan, S. Raffy, M.A. Oturan, Development of Ti/TiO_x foams for removal of organic pollutants from water: Influence of porous structure of Ti substrate, Appl. Catal. B Environ. 317 (2022), 121736, https://doi.org/10.1016/j.apcatb.2022.121736.
[41] S. Nayak, B.P. Chaplin, Fabrication and characterization of porous, conductive, monolithic Ti_4O_7 electrodes, Electrochim. Acta 263 (2018) 299–310, https://doi.org/10.1016/j.electacta.2018.01.034.
[42] Y. Wang, L. Li, Y. Wang, H. Shi, L. Wang, Q. Huang, Electrooxidation of perfluorooctanesulfonic acid on porous Magnéli phase titanium suboxide Anodes: Impact of porous structure and composition, Chem. Eng. J. 431 (2022), 133929, https://doi.org/10.1016/j.cej.2021.133929.
[43] N. Krstajic, S. Trasatti, Cathodic behaviour of RuO2-doped Ni/Co3O4 electrodes in alkaline solutions: hydrogen evolution, J. Appl. Electrochem. 28, 1291–1297. https://doi.org/10.1023/A:1003444110172.
[44] A. Kapałka, G. Fóti, C. Comninellis, Determination of the Tafel slope for oxygen evolution on boron-doped diamond electrodes, Electrochem. Commun. 10 (2008) 607–610, https://doi.org/10.1016/j.elecom.2008.02.003.
[45] L.A.D. Faria, Electrocatalytic properties of ternary oxide mixtures of composition $Ru_{0.3}Ti_{(0.7-x)}Ce_xO_z$: oxygen evolution from acidic solution, J. Appl. Electrochem. 26, 1195–1199. https://doi.org/10.1007/BF00243745.
[46] J.O. Bockris, T. Otagawa, The Electrocatalysis of Oxygen Evolution on Perovskites, J. Electrochem. Soc. 131 (1984) 290–302, https://doi.org/10.1149/1.2115565.
[47] Y.-J. Shih, C.-P. Huang, Y.-H. Chan, Y.-H. Huang, Electrochemical degradation of oxalic acid over highly reactive nano-textured γ- and α-MnO2/carbon electrode fabricated by KMnO4 reduction on loofah sponge-derived active carbon, J. Hazard. Mater. 379 (2019), 120759, https://doi.org/10.1016/j.jhazmat.2019.120759.
[48] Y. Jing, B.P. Chaplin, Mechanistic Study of the Validity of Using Hydroxyl Radical Probes To Characterize Electrochemical Advanced Oxidation Processes, Environ. Sci. Technol. 51 (2017) 2355–2365, https://doi.org/10.1021/acs.est.6b05513.
[49] J. Ma, C. Trellu, N. Oturan, S. Raffy, M.A. Oturan, Porous Magnéli phase obtained from 3D printing for efficient anodic oxidation process, Chem. Eng. J. 456 (2023), 141047, https://doi.org/10.1016/j.cej.2022.141047.
[50] Z. Zhao, J. Zhang, J. Yao, S. You, Electrochemical removal of 4-chlorophenol in water using a porous Magnéli-phase (Ti_4O_7) electrode, Environ. Res. 210 (2022), 113004, https://doi.org/10.1016/j.envres.2022.113004.
[51] A.S. Malik, T. Liu, M. Dupuis, R. Li, C. Li, Water Oxidation on TiO_2: A Comparative DFT Study of $1e^-$, $2e^-$, and $4e^-$ Processes on Rutile, Anatase, and Brookite, J. Phys. Chem. C. 124 (2020) 8094–8100, https://doi.org/10.1021/acs.jpcc.9b11450.
[52] J. Xie, C. Zhang, T.D. Waite, Hydroxyl radicals in anodic oxidation systems: generation, identification and quantification, Water Res 217 (2022), 118425, https://doi.org/10.1016/j.watres.2022.118425.
[53] J. Qi, W. Zhang, R. Cao, Porous Materials as Highly Efficient Electrocatalysts for the Oxygen Evolution Reaction, ChemCatChem 10 (2018) 1206–1220, https://doi.org/10.1002/cctc.201701637.
[54] L. Xu, Q. Jiang, Z. Xiao, X. Li, J. Huo, S. Wang, L. Dai, Plasma-Engraved Co_3O_4 Nanosheets with Oxygen Vacancies and High Surface Area for the Oxygen Evolution Reaction, Angew. Chem. Int. Ed. 55 (2016) 5277–5281, https://doi.org/10.1002/anie.201600687.
[55] B. Šljukić, R. Baron, R.G. Compton, Electrochemical Determination of Oxalate at Pyrolytic Graphite Electrodes, Electroanalysis 19 (2007) 918–922, https://doi.org/10.1002/elan.200703852.
[56] P. Gayen, C. Chen, J.T. Abiade, B.P. Chaplin, Electrochemical Oxidation of Atrazine and Clothianidin on Bi-doped SnO_2-Ti_nO_{2n-1} Electrocatalytic Reactive Electrochemical Membranes, Environ. Sci. Technol. 52 (2018) 12675–12684, https://doi.org/10.1021/acs.est.8b04103.
[57] D. Maggiolo, F. Picano, F. Zanini, S. Carmignato, M. Guarnieri, S. Sasic, H. Ström, Solute transport and reaction in porous electrodes at high Schmidt numbers, J. Fluid Mech. 896 (2020), A13, https://doi.org/10.1017/jfm.2020.344.